

## Synthesis and Characterization of Pt–V–SnO<sub>2</sub>/C Electrocatalysts for Ethanol Oxidation in Acidic Media

Hongyan Sun, Lianhua Zhao\*, Fengchun Yu

Department of Chemistry, College of Science, Yanbian University, Yanji 133002, Jilin, China.

\*E-mail: [zhaolianhua@ybu.edu.cn](mailto:zhaolianhua@ybu.edu.cn)

Received: 26 December 2012 / Accepted: 20 January 2013 / Published: 1 February 2013

---

A series of Pt, Pt–V, Pt–SnO<sub>2</sub> and Pt–V–SnO<sub>2</sub> anode electrocatalysts have been synthesized by a modified Bönemann method on carbon Vulcan XC-72 and characterized by XRD, HR–TEM, EDS and XPS. The XRD and HR–TEM analyses reveal two phases in the ternary Pt–V–SnO<sub>2</sub>/C catalyst: solid solution of V in Pt and SnO<sub>2</sub>. The addition of Sn and V is found to change the geometric and electronic structure of Pt. The electrochemical properties of these materials as a function of their composition have been measured in 0.5 M H<sub>2</sub>SO<sub>4</sub> solution containing 0.5 M C<sub>2</sub>H<sub>5</sub>OH by linear sweep voltammetry, chronoamperometry and electrochemical impedance spectra. The catalytic activity of the electrocatalysts for ethanol oxidation reaction (EOR) is in the order Pt–V–SnO<sub>2</sub>/C > Pt–V/C > Pt–SnO<sub>2</sub>/C > Pt/C. Analysis of the electrochemical data suggests that the incorporation of V into Pt–SnO<sub>2</sub> enhances the catalytic activity for EOR.

---

**Keywords:** Pt–V–SnO<sub>2</sub>/C nanocatalyst; Ethanol electrooxidation; Direct ethanol fuel cell; Bönemann method.

### 1. INTRODUCTION

Fuel cells that directly convert liquid fuels such as methanol or ethanol at low temperatures are probably the most viable means for powering portable devices. In particular, methanol has been extensively studied as the fuel for direct fuel cells for mobile applications [1–3]. Methanol is preferred over hydrogen because it is a liquid and thus its transport, storage and handling are much easier. However, methanol is a neurotoxin and its high miscibility with water [4] could lead to potential environmental issues. The fuel cell community is now looking at ethanol as an alternative to methanol. Compared with methanol, ethanol has high theoretical mass energy density [5], can be produced from biomass through fermentation, and has much less toxicity [6, 7]. In principle, the use of ethanol as a fuel would not significantly alter the natural balance of carbon dioxide in the atmosphere, as the carbon dioxide released from the fuel cell is reused by the biomass. However, the fuel cell performance and

efficiency are hindered due to various limiting factors under the operating conditions. One of the issues is the sluggish kinetics of the oxygen reaction at the anode side. Compared with methanol, it is much more difficult to completely oxidize ethanol to  $\text{H}_2\text{O}$  and  $\text{CO}_2$  because of the C–C bond in ethanol, which leads to poor cell performance. Thus, it has been a challenge to find an efficient catalyst to increase the electroreactivity of ethanol.

Pt was recognized to be the most active catalyst for the ethanol oxidation reaction (EOR). However, it is readily poisoned by adsorbed CO species and does not easily provoke C–C bond breaking for complete oxidation of ethanol. On the basis of these investigations and in the context of the EOR mechanisms, EOR activity could be enhanced by (i) modification of the electronic structure of Pt (5d-band vacancies), (ii) changes in the physical structure of Pt (Pt–Pt bond distance and coordination number), (iii) adsorption of oxygen-containing species (oxygen or hydroxyl species) from the electrolyte on the Pt or alloying element [8]. Among the Pt-based alloy catalysts Pt–M (M = Ru, Sn, Re, Rh, Pd, V, etc.) [9, 10], Pt–Sn/C has been the most active for EOR, which increases the current density and decreases the onset potential of ethanol oxidation by approximately 0.2 V compared with using Pt alone. Sn is able to adsorb water molecules dissociatively to form  $\text{OH}_{\text{ads}}$  species, which results in the formation of  $\text{CO}_2$  and  $\text{CH}_3\text{COOH}$  at lower potentials than Pt by oxidation of adsorbed CO and  $\text{CH}_3\text{CO}$  species, according to the bifunctional mechanism [11]. However, the experimental results show that ethanol is still not completely oxidized to  $\text{CO}_2$  on the Pt–Sn/C anode [12,13].

Usually, the addition of precious metals as a third element to the Pt–Sn bimetallic catalyst can enhance EOR activity at low temperature and lead to complete oxidation of ethanol, as demonstrated in the Pt–M–Sn/C example catalysts (M = Ru, Rh, Re, Ir, Pd, Ni, Mo, etc.) [14–20]. Kowal et al. [15] showed that in heterogeneous catalysis, the additional of Rh as the third element to Pt–Sn resulted in a good catalyst that not only increased the EOR activity but also assisted the C–C bond breakage. Zhao et al. [17] prepared Pt–Ir– $\text{SnO}_2$ /C catalysts that also showed similar effects. In this work, V was used as the third metal to incorporate into Pt– $\text{SnO}_2$  catalysts.  $\text{V}_2\text{O}_5$  has been extensively used as cathode in lithium ion batteries [21], and the vanadium(IV)/vanadium(III) redox couple has been used to construct a redox type fuel cell [22]. Maiyalagan et al. [23] reported Pt/ $\text{V}_2\text{O}_5$ –C composite as a good anode catalyst for methanol. Besides, vanadium is much cheaper than the platinum group elements. To our knowledge, there has been no report on the catalytic activity of Pt–V– $\text{SnO}_2$ /C ternary catalyst for EOR. Accordingly, we present here the synthesis and characterization of Pt–V– $\text{SnO}_2$ /C and its potential as an alternative anode catalyst for DEFC. The Pt/C, Pt–V/C, Pt– $\text{SnO}_2$ /C and Pt–V– $\text{SnO}_2$ /C catalysts were prepared by the modified Bönemann method [24] to obtain supported nanoparticles with high loading on carbon. To study the effect of V addition to Pt–Sn, the atomic ratio of Pt:Sn was fixed at 1:1 for all of the samples tested.

## 2. EXPERIMENTAL

### 2.1. Catalysts preparation

The carbon-supported catalysts with 60 wt% metal loading were synthesized by a slightly modified Bönemann method [24] as described below.  $\text{N}(\text{Oct})_4(\text{BEt}_3\text{H})$  dissolved in tetrahydrofuran

(>99.5%, 100 mL) was added to a tetrahydrofuran solution containing  $\text{PtCl}_2$  (0.1330 g),  $\text{SnCl}_2$  (0.0967 g), and  $\text{VCl}_3$  (0.0265 g) with vigorous stirring at 30 °C under a nitrogen atmosphere. After 1.5 h, the reaction mixture turned into a colloidal suspension, and high surface area carbon (Vulcan XC-72, 0.1103 g) was added. The suspension was then kept at 30 °C overnight. The catalyst were collected by filtration, washed thoroughly with water, dried in air (40–50 °C), and the powder was then further calcified at 300 °C in air. Three Pt–V– $\text{SnO}_2$ /C catalysts with a Pt/V/Sn atomic ratio of 1:(1/4):1, 1:(1/3):1 and 1:(2/3):1 were obtained respectively.

The same procedure was repeated for the preparation of Pt/C, Pt–V/C and Pt– $\text{SnO}_2$ /C catalysts (in the absence of the corresponding catalysts) to allow the comparison between the Pt/C, Pt–V/C, Pt– $\text{SnO}_2$ /C and Pt–V– $\text{SnO}_2$ /C systems.

## 2.2. Catalysts characterizations

Crystallographic phase analysis was carried out using X-ray diffraction (XRD, Max-C, Rigaku) and the spectrometer was equipped with a  $\text{Cu } K_\alpha$  radiation source. The lattice parameters were obtained by fitting the Pt (220) XRD diffraction peak with the pseudo-Voigt function, assuming that the Pt (220) surface is free from the impact of carbon and the  $\text{SnO}_2$  crystal face. Catalyst nanoparticles deposited on high surface area carbon were examined by high resolution transmission electron microscopy (HR-TEM) using Tecnai G2 F20 S-Twin transmission electron microscope with a field emission gun at 200 kV ( Philips-FEI). The atomic ratio of Pt, V, and Sn metals on carbon were measured by energy dispersive spectroscopy (EDS) attached to a scanning electron microscope (SEM, HITACHI-S4800). X-ray photoelectron spectroscopy (XPS, Lb250 UK) data were used to determine the oxidation states of Pt on the surface layers of the samples.

## 2.3. Electrochemical measurements

The electrochemical characterizations were conducted with a CHI-660D electrochemical analyzer in a conventional single-compartment three-electrode cell with a platinum foil counter electrode. A saturated calomel electrode (SCE) in a saturated KCl solution served as the reference electrode. A glassy carbon (3 mm dia.) electrode was polished to a mirror-like finish with 1.0, 0.3, 0.05  $\mu\text{m}$  alumina media, respectively, and coated with a thin layer of the catalyst to serve as the working electrode. In a typical experiment, the catalyst ink was prepared by dispersing 5 mg catalyst in 0.5 mL isopropanol and 50 mg 5 wt% Nafion solution under ultrasonic vibration for 10 min. When a dark homogeneous dispersion was formed, 7.5  $\mu\text{L}$  of the ink was dropped onto the glassy carbon electrode and dried in air to give an effective catalyst loading of 1  $\text{mg cm}^{-2}$ . The linear sweep voltammetry (LSV), chronoamperometry (CA) and electrochemical impedance spectra (EIS) experiments were performed using 0.5 M  $\text{H}_2\text{SO}_4$  solution containing 0.5 M  $\text{C}_2\text{H}_5\text{OH}$  at 30 °C. The EIS were measured over a frequency range between 100 kHz and 10 MHz applying a single sine wave of 5 mV amplitude. The impedance values were normalized by geometric electrode surface area. All

solutions were prepared with high purity water and deaerated by  $N_2$  before the electrochemical measurements.

### 3. RESULTS AND DISCUSSION

#### 3.1. Physicochemical characterization

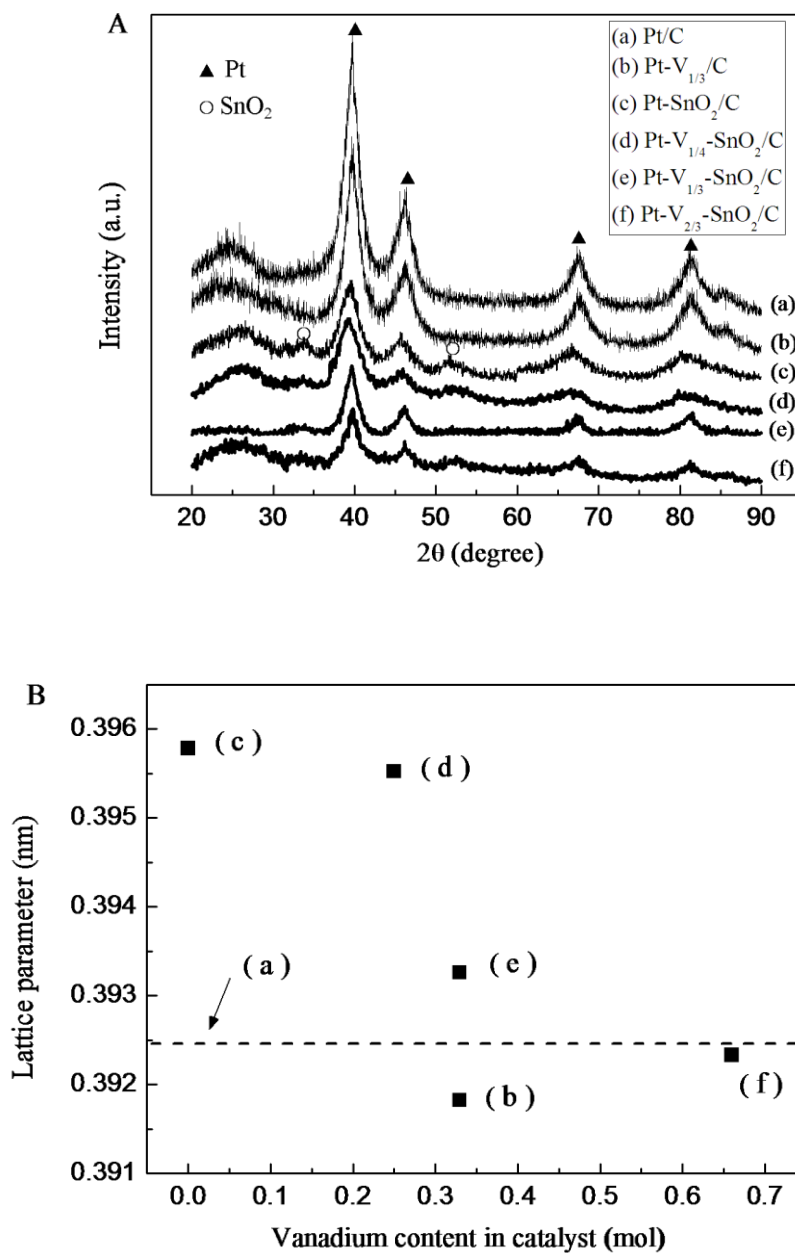


**Figure 1.** XRD patterns of different Pt-based catalysts (A) and dependence of the FCC lattice parameter of the catalysts on V content (B).

Figure 1A shows the XRD patterns of Pt/C, Pt-V<sub>1/3</sub>/C, Pt-SnO<sub>2</sub>/C, and Pt-V<sub>x</sub>-SnO<sub>2</sub>/C ( $x = 1/4, 1/3, 2/3$ ) catalysts. The peak at 20°–30° observed in all diffraction patterns of the carbon supported catalysts is attributed to the (002) plane of the hexagonal structure of Vulcan XC-72 carbon support. The diffraction peaks at around 39°, 46°, 67° and 82° are attributed to Pt (111), (200), (220) and (311) crystalline planes respectively, which represent the typical character of crystalline Pt with face centered cubic (FCC) crystalline structure. Small diffraction peaks can be observed at around 34° and 52° in Pt-SnO<sub>2</sub>/C and Pt-V-SnO<sub>2</sub>/C catalysts, which are associated with the (101) and (211) planes of tetragonal SnO<sub>2</sub>. Because the lattice parameter of Pt will change if metallic V or Sn form an alloy with Pt, the lattice parameter of the catalyst is calculated from Bragg's equation based on Pt (220) peaks [25]. Figure 1B shows that the Pt (220) facets of Pt/C (0.3924 nm), Pt-V/C (0.3918 nm), Pt-V<sub>1/4</sub>-SnO<sub>2</sub>/C (0.3955 nm), Pt-V<sub>1/3</sub>-SnO<sub>2</sub>/C (0.3933 nm) and Pt-V<sub>2/3</sub>-SnO<sub>2</sub>/C (0.3923 nm) are smaller than that of Pt-SnO<sub>2</sub>/C (0.3958 nm). This might be due to the incorporation of a larger Sn ( $R_{\text{Sn}} = 0.155$  nm, value determined from interatomic distances in alloys with appropriate structure) [26] for Pt ( $R_{\text{Pt}} = 0.139$  nm). On the other hand, the reflections of Pt-V/C and Pt-V-SnO<sub>2</sub>/C shift to higher  $2\theta$  values compared to those of Pt-SnO<sub>2</sub>/C due to the substitution of smaller V ( $R_{\text{V}} = 0.131$  nm)[27] for Sn.

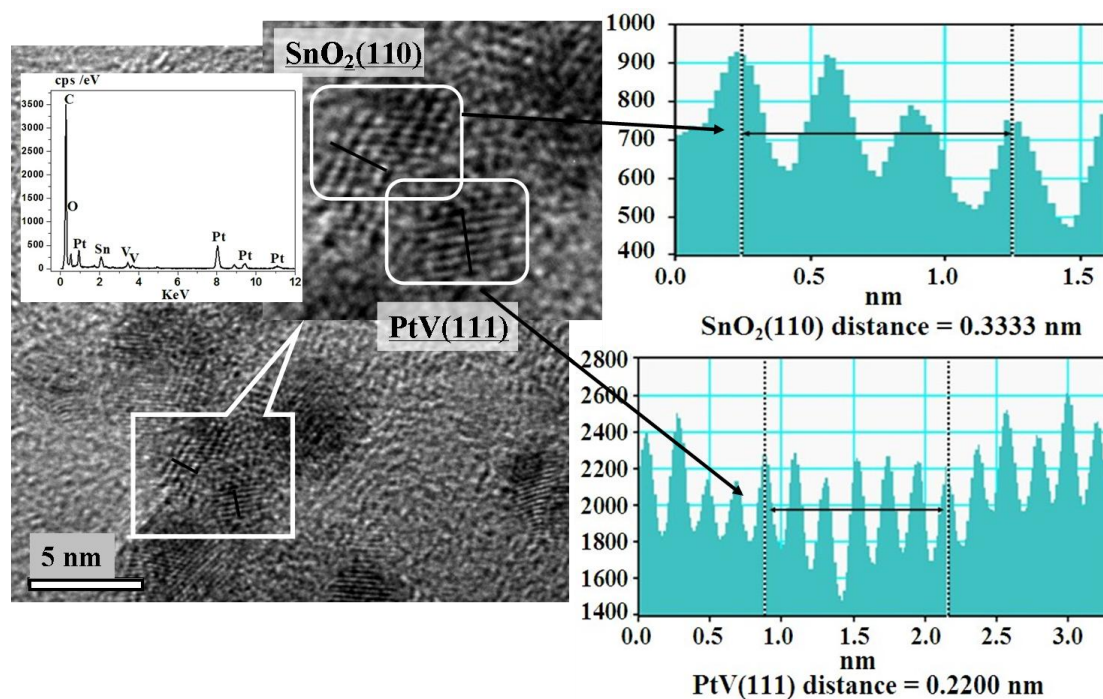


**Figure 2.** EDS and HR-TEM image of Pt-V<sub>1/3</sub>-SnO<sub>2</sub>/C and pixel intensity profiles for the SnO<sub>2</sub> and Pt-V crystallites.

All the catalysts were examined by HR-TEM imaging. Figure 2 shows image of Pt-V<sub>1/3</sub>-SnO<sub>2</sub>/C. In the high magnification image of a cluster of two metallic phases, their lattices can be observed in the bright field due to the phase contrast. Pixel intensity profile of the wider cluster reveals that the distance between the adjacent fringes is 0.3333 nm, which corresponds to the interplanar

distance of the tetragonal  $\text{SnO}_2$  (110),  $d_{110} = 0.3353$  nm. For the narrower cluster, the pixel intensity profile indicates an average distance of 0.2200 nm between the adjacent fringes, which is close to the interplanar distance of FCC Pt–V (111),  $d_{111} = 0.2240$  nm [28]. Particle size analysis shows that the diameter of Pt–V<sub>1/3</sub>–SnO<sub>2</sub>/C is in the range of 2–5 nm.

**Table 1.** Compositional characterization of electrocatalysts.

Electrocatalyst	Nominal composition (Pt/V/Sn atom ratio)	EDS composition (Pt/V/Sn atom ratio)	TEM particle size (nm)
Pt/C	100:0:0	100:0:0	3.49
Pt-V <sub>1/3</sub> /C	75:25:0	75.3:24.7:0	4.34
Pt-SnO <sub>2</sub> /C	50:0:50	55.7:0:44.3	3.11
Pt-V <sub>1/4</sub> -SnO <sub>2</sub> /C	44.4:11.2:44.4	50.2:13.8:36.0	3.19
Pt-V <sub>1/3</sub> -SnO <sub>2</sub> /C	42.9:14.2:42.9	45.4:14.8:39.8	3.33
Pt-V <sub>2/3</sub> -SnO <sub>2</sub> /C	37.5:25.0:37.5	34.5:27.7:37.8	4.42

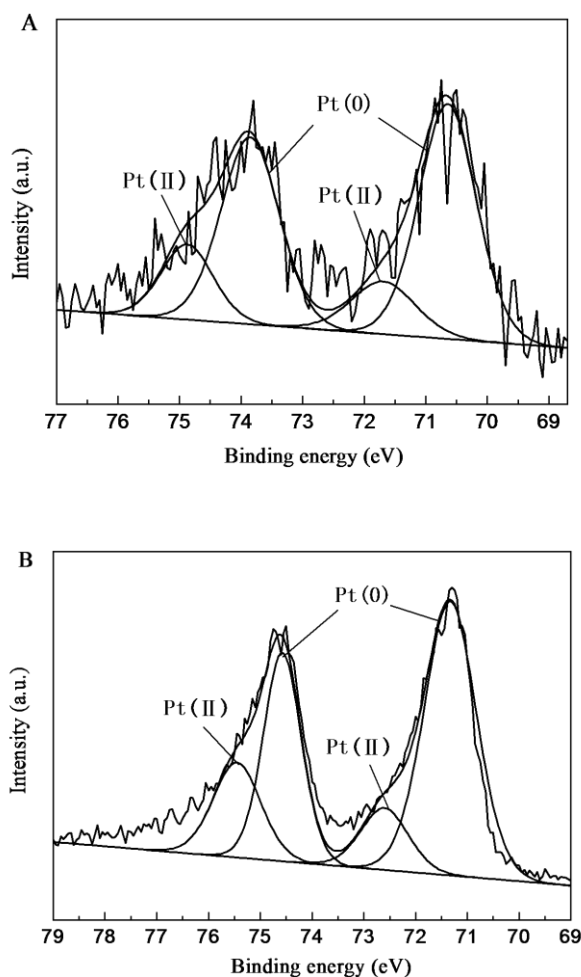


**Figure 3.** Pt 4f XPS spectra of Pt–V<sub>1/3</sub>–SnO<sub>2</sub>/C (A) and Pt-SnO<sub>2</sub>/C (B).

The EDS analysis of all Pt–V<sub>x</sub>–SnO<sub>2</sub>/C catalysts indicates the presence of Pt, V, Sn and carbon. The synthesized catalysts have atomic compositions similar to the nominal values, as listed in Table 1.

The oxidation states of Pt in the surface layers of the catalyst nanoparticles were examined by XPS. Figure 3 shows the Pt 4f XPS spectra of the Pt–V<sub>1/3</sub>–SnO<sub>2</sub>/C (A) and Pt–SnO<sub>2</sub>/C (B) samples. The addition of V caused redshifts for the Pt(0) and Pt(II) peaks at 0.69 eV and 0.72 eV in sample (A), and redshifts at 0.91 eV and 0.57 eV in sample (B), respectively. The shift of the binding energy of Pt indicates that the electronic structure of the Pt in Pt–V<sub>1/3</sub>–SnO<sub>2</sub>/C might be changed due to the addition of V.

### 3.2. Ethanol electrooxidation activity

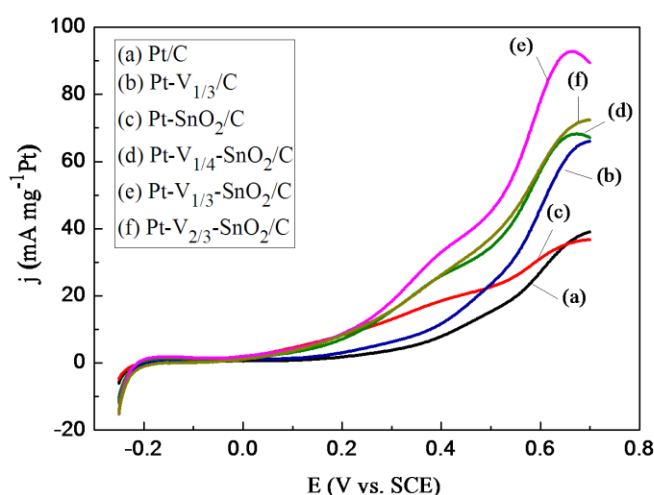


**Figure 4.** Anodic sweep curves of the cyclic voltammetry, comparing activity of different catalysts for the ethanol oxidation reaction. Reaction conditions: 0.5 M H<sub>2</sub>SO<sub>4</sub> + 0.5 M C<sub>2</sub>H<sub>5</sub>OH solution. Scan rate 10 mVs<sup>-1</sup>, 30 °C.

The ethanol electrooxidation activity of the synthesized catalysts was characterized by LSV in 0.5 M H<sub>2</sub>SO<sub>4</sub> solution containing 0.5 M ethanol with a potential range between –0.25 and 0.7 V at 30 °C (Figure 4). The specific activity of the catalysts for the EOR is in the order Pt–V<sub>1/3</sub>–SnO<sub>2</sub>/C > Pt–V<sub>2/3</sub>–SnO<sub>2</sub>/C ≈ Pt–V<sub>1/4</sub>–SnO<sub>2</sub>/C > Pt–V<sub>1/3</sub>/C > Pt–SnO<sub>2</sub>/C > Pt/C. The addition of SnO<sub>2</sub> to Pt improves the EOR kinetics, which can provide OH species for the removal of poisonous intermediates according to the bifunctional mechanism at low potential [29]. The EOR activity of Pt–V<sub>x</sub>–SnO<sub>2</sub>/C ( $x = 1/4, 1/3, 2/3$ ) is superior to that of Pt–SnO<sub>2</sub>/C. In particular, the Pt–V<sub>1/3</sub>–SnO<sub>2</sub>/C catalyst gave the lowest onset potential but the highest current within the potential range between 0.2 and 0.7 V. In our case, the high EOR activity of the Pt–V<sub>1/3</sub>–SnO<sub>2</sub>/C catalyst might also be due to changes in the surface morphology and the electronic structure of the catalysts upon loading a small amount of vanadium. This kind of phenomenon can be interpreted based on a synergistic effect between Sn and V. The observed current

density of the catalysts is similar to other Pt-based catalysts (such as Pt–M–Sn/C, M = Ru, Rh, Re, Ir, Pd, Ni, Mo etc.) that were evaluated under the same experimental conditions [14–20].

To evaluate both the EOR activity and the stability of the active sites under continuous operation conditions, CA was carried out at 0.5 V for 3 h. In all six CA curves shown in Figure 5, the mass current decay curves have a holding potential of 0.5 V at 30 °C for the EOR in 0.5 M H<sub>2</sub>SO<sub>4</sub> containing 0.5 M ethanol.

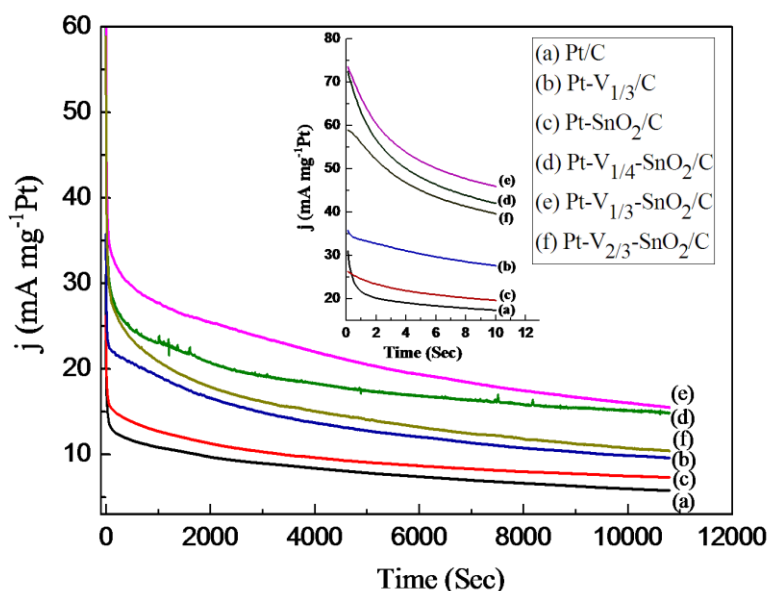


**Figure 5.** Chronoamperometry curves for the ethanol oxidation reaction on different catalysts, recorded in 0.5 M H<sub>2</sub>SO<sub>4</sub> + 0.5 M C<sub>2</sub>H<sub>5</sub>OH electrolyte, at 0.5 V, 30 °C.

The current drops continuously with time and after some time it becomes relatively stable. The current value may decay due to poisoning of surface active sites and the instability of catalyst particles. The binary Pt–SnO<sub>2</sub>/C catalyst showed better performance than pure Pt/C, which confirms the benefit for the EOR by adding SnO<sub>2</sub> to Pt [30]. The ternary Pt–V<sub>x</sub>–SnO<sub>2</sub>/C ( $x = 1/4, 1/3, 2/3$ ) catalysts gave higher current than the binary Pt–V<sub>1/3</sub>/C and Pt–SnO<sub>2</sub>/C catalysts. The higher current obtained for the ternary catalysts may be explained by the synergistic effect between Sn and V. This may indicate an increase in structural defects or roughness, making the ternary catalysts better candidates for ethanol electrooxidation [31].

Figure 6 compares the EIS for EOR on the Pt–SnO<sub>2</sub>/C and Pt–V<sub>1/3</sub>–SnO<sub>2</sub>/C catalysts at the electrode potentials of 0.3 and 0.5 V. At 0.3 V, a large arc is seen in the spectrum of each catalyst. This reveals slow reaction kinetics for ethanol dehydrogenation caused by strongly adsorbed intermediate species such as CH<sub>x</sub> or CO [32]. They are adsorbed on the Pt sites and they block the continuous adsorption of ethanol molecules. With increasing potential, the reaction kinetics becomes faster and the diameter of the arc decreases to form a semicircle. At 0.5 V, which is high enough for some of the adsorbed intermediate species to be oxidized with the increased supply of oxygen containing species, fresh Pt sites for further ethanol adsorption are exposed [33–35]. The diameter of the semicircle at high

frequency is related to the charge transfer resistance of the catalyst toward the oxidation of ethanol, and it can be used to compare the activities of different catalysts. As can be seen from Figure 6, the charge transfer resistance of Pt-V<sub>1/3</sub>-SnO<sub>2</sub>/C is lower than that of Pt-SnO<sub>2</sub>/C at all of the tested potentials. This indicates that the ternary catalyst is more tolerant to the intermediate species poisoning at lower potentials and the EOR is faster on Pt-V<sub>1/3</sub>-SnO<sub>2</sub>/C compared to that on Pt-SnO<sub>2</sub>/C.

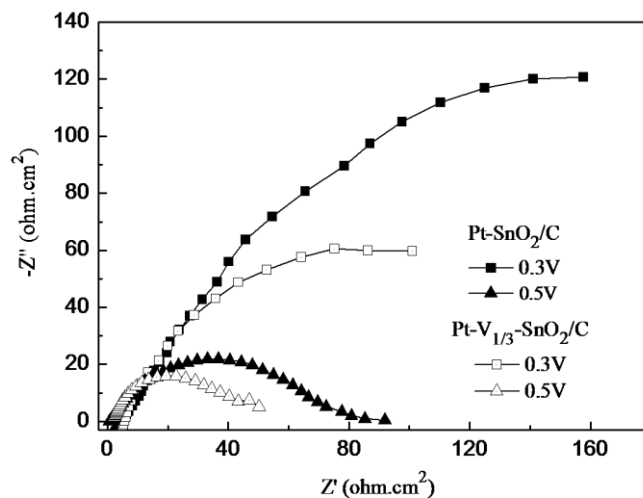


**Figure 6.** Complex-plane impedance plots of Pt-SnO<sub>2</sub>/C and Pt-V<sub>1/3</sub>-SnO<sub>2</sub>/C in 0.5 M H<sub>2</sub>SO<sub>4</sub> + 0.5 M C<sub>2</sub>H<sub>5</sub>OH electrolyte at various electrode potentials, at 30 °C.

#### 4. CONCLUSIONS

The ternary Pt-V-SnO<sub>2</sub>/C electrocatalysts were synthesized by a modified Bönemann method and evaluated for ethanol oxidation. XRD and HR-TEM analysis revealed two phases: solid solution of V in Pt and SnO<sub>2</sub>. The activity of Pt-V<sub>1/3</sub>-SnO<sub>2</sub>/C for EOR was found to be higher than that of Pt/C, Pt-V/C and Pt-SnO<sub>2</sub>/C catalysts. It was proven that trifunctional catalyst is necessary for efficient EOR. It can be seen from the electrochemical data that the oxide phases promote the EOR, and the incorporation of a small amount of V into Pt-SnO<sub>2</sub>/C might change the geometric and electronic structure of the Pt in Pt-V<sub>1/3</sub>-SnO<sub>2</sub>/C and further enhance the EOR activity. In the future, we will also further study the reaction mechanism.

#### ACKNOWLEDGEMENTS

This work was financially supported by the Jilin Provincial Science and Technology Project of China (No. 20120741).

#### References

1. C. Lamy, E.M. Belgsir and J.M. L'eger, *J. Appl. Electrochem.* 31 (2001) 799.
2. A. Serov and C. Kwak, *Appl. Catal. B: Environ.* 90 (2009) 313.
3. W.J. Zhou, B. Zhou, W.Z. Li, Z.H. Zhou, S.Q. Song, G.Q. Sun, Q. Xin, S. Douvartzides, M. Goula

- and P. Tsiakaras, *J. Power Sources*. 126 (2004) 16.
4. C. Lamy, S. Rousseau, E.M. Belgsir, C. Coutanceau and J.M. Leger, *Electrochimica. Acta*. 49 (2004) 3901.
  5. F. Vigier, C. Coutanceau, A. Perrard, E.M. Belgsir and C. Lamy, *J. Appl. Electrochem.* 34 (2004) 439.
  6. S. Topcagic and S.D. Minteer, *Electrochim Acta*. 51 (2006) 2168.
  7. E. Antolini, *J. Power Sources*. 170 (2007) 1–12.
  8. C.V. Rao and B. Viswanathan, *J. Phys. Chem. C* 113 (2009) 18907.
  9. Z.F. Xu and Y.X. Wang, *J. Phys. Chem. C* 115 (2011) 20565.
  10. G. Corbel, M. Topic, A. Gibaud, C.I. Lang, *J. Alloy. Compd.* 509 (2011) 6532.
  11. W.J. Zhou, W.Z. Li, S.Q. Song, Z.H. Zhou, L.H. Jiang and G.Q. Sun, et al. *J. Power Sources*. 131 (2004) 217.
  12. M. Zhu, G. Sun and Q. Xin, *Electrochim Acta*. 54 (2009) 1511.
  13. J.M.S. Ayoub, R.F.B. De Souza, J.C.M. Silva, R.M. Piasentin, E.V. Spinacé, M.C. Santos and A.O. Neto, *Int. J. Electrochem. Sci.* 7 (2012) 11351.
  14. T. Takeguchi, G.X. Wang, E.N. Muhamad and W. Ueda, *ECS Transactions* 16 (2008) 713.
  15. A. Kowal, M. Li, M. Shao, K. Sasaki, M.B. Vukmirovic, J. Zhang, N.S. Marinkovic, P. Liu, A.I. Frenkel and R.R. Adzic, *Nat Mater.* 8 (2009) 325.
  16. J. Tayal, B. Rawat and S. Basu, *Int. J. Hydrogen Energy*. 37 (2012) 4597.
  17. L.H. Zhao, S. Mitsushima, A. Ishihara, K. Matsuzawa and K. Ota, *Chin. J. Catal.* 32 (2011) 1856.
  18. E. Lee, I.S. Park and A. Manthiram, *J. Phys. Chem. C* 114 (2010) 10634.
  19. Patri'cia dos Santos Correa and Elen Leal da Silva, et al. *Int. J. Hydrogen Energy* 37 (2012) 9314.
  20. E. Lee, A. Murthy and A. Manthiram, *Electrochim Acta* 56 (2011)1611.
  21. Y. Wang and G.Z. Cao, *Adv Mater* 20 (2008) 2251.
  22. B. Folkesson and R. Larsson, *Inorg. Chim. Acta*. 162 (1989)75.
  23. T. Maiyalagan and F. Nawaz Khan, *Catal. Commun.* 10 (2009) 433.
  24. H. Bönemann, W. Brijujoux, R. Brinkmann, E. Dinjus, T. Jousen and B. Korall, *Angew Chem. Int. Ed. Engl.* 30 (1991) 1312.
  25. V. Radmilovic, H.A. Gasteiger and P.N. Ross, *J. Catal.* 154 (1995) 98.
  26. R.J.D. Tilley, *Understanding Solids: The Science of Materials*; John Wiley & Sons: Chichester, 2005.
  27. A. Gibaud, M. Topić, G. Corbel and C.I. Lang, *J. Alloy. Compd.* 484 (2009) 168.
  28. G. Cambanis and D. Chadwick, *Appl. Catal.* 25 (1986) 191.
  29. Q. Wang, G.Q. Sun, L.H. Jiang, Q. Xin, S.G. Sun, Y.X. Jiang, S.P. Chen, Z. Jusys and R.J. Behm, *Phys. Chem. Chem. Phys.* 9 (2007) 2686.
  30. L.H. Jiang, G.Q. Sun, S.G. Sun, J.G. Liu, S.H. Tang, H.Q. Li, B. Zhou and Q. Xin, *Electrochim. Acta*. 50 (2005) 5384.
  31. G.A. Somorjai, *J. Phys. Chem.* 94 (1990) 1013.
  32. F. Vigier, C. Coutanceau, A.Perrard, E.M. Belgsir and C. Lamy, *J. Appl. Electrochem.* 34 (2004) 439.
  33. F. Seland, R. Tunold and D.A. Harrington, *Electrochim. Acta*. 51 (2006) 3827.
  34. W. Sugimoto, K. Aoyama, T. Kawaguchi, Y. Murakami and Y. Takasu, *J. Electroanal. Chem.* 576 (2005) 215.
  35. P. Bommersbach, M. Mohamedi and D. Guay, *J. Electrochem. Soc.* 154 (2007) B876.